Title

Activity-dependent Protein Dynamics Define Interconnected Cores of Co-regulated Postsynaptic Proteins*

Journal

Molecular & Cellular Proteomics, 12(1)

ISSN

1535-9476

Authors

Trinidad, Jonathan C
Thalhammer, Agnes
Burlingame, Alma L
et al.

Publication Date

2013

DOI

10.1074/mcp.m112.019976

Peer reviewed

Activity-dependent Protein Dynamics Define Interconnected Cores of Co-regulated Postsynaptic Proteins*[S]

Jonathan C. Trinidad‡§, Agnes Thalhammer§¶, Alma L. Burlingame‖‡, and Ralf Schoepfer‖¶

Synapses are highly dynamic structures that mediate cell–cell communication in the central nervous system. Their molecular composition is altered in an activity-dependent fashion, which modulates the efficacy of subsequent synaptic transmission events. Whereas activity-dependent trafficking of individual key synaptic proteins into and out of the synapse has been characterized previously, global activity-dependent changes in the synaptic proteome have not been studied.

To test the feasibility of carrying out an unbiased large-scale approach, we investigated alterations in the molecular composition of synaptic spines following mass stimulation of the central nervous system induced by pilocarpine. We observed widespread changes in relative synaptic abundances encompassing essentially all proteins, supporting the view that the molecular composition of the postsynaptic density is tightly regulated. In most cases, we observed that members of gene families displayed coordinate regulation even when they were not known to physically interact.

Analysis of correlated synaptic localization revealed a tightly co-regulated cluster of proteins, consisting of mainly glutamate receptors and their adaptors. This cluster constitutes a functional core of the postsynaptic machinery, and changes in its size affect synaptic strength and synaptic size. Our data show that the unbiased investigation of activity-dependent signaling of the postsynaptic density proteome can offer valuable new information on synaptic plasticity. ***Molecular & Cellular Proteomics 12: 10.1074/mcp.M112.019976, 29–41, 2013.***

Excitatory synaptic transmission is the primary mode of cell–cell communication in the central nervous system. The efficacy of synaptic transmission is highly regulated, and alterations in the strength of synaptic signaling within networks of neurons provide a mechanism for learning and memory storage, as well as for overall network stability. Modulation of synapse efficacy can occur through alterations in the structure and composition of the postsynaptic spine. The synaptic abundance of several molecules has been shown to be regulated in response to activity (1).

The levels of individual proteins at postsynaptic spines are regulated through multiple processes. Active transport mechanisms exist and have been well characterized for AMPA-type glutamate receptors (AMPA-Rs)[1] via either insertion into the synapse or tighter association with the postsynaptic density (PSD) following lateral diffusion within the cell membrane (2). In addition to AMPA-Rs, other proteins known to be subject to activity-dependent regulation include calcium calmodulin-dependent protein kinase II alpha and beta, NMDA-type glutamate receptors (NMDA-Rs), and proteosome subunits (3–5). Synaptic protein content is dysregulated in a number of neuropsychiatric and neurodegenerative diseases, including Alzheimer's disease and fragile X mental retardation (6–8).

Most studies reported thus far have focused on a small number of selected molecules in individual experiments using a subset of synapses. Whereas learning and memory rely on the differential response of individual synapses to their specific input patterns, overall network excitability has to be maintained by homeostatic means. This homeostasis is governed by multiple pathways, and very little is known about the principles that regulate synaptic protein content across large numbers of synapses and neurons. The contributions of individual pathways and the interactions among them are largely unknown.

In order to explore synaptic dynamics with a global view, we took advantage of a chemically induced mass stimulation protocol to stimulate synapses broadly throughout the central nervous system. We employed mass spectrometry and isotopically encoded isobaric peptide tagging with the iTRAQ reagent to quantify changes in the abundance of 893 proteins (9). We then analyzed changes in the relative abundance of

From the ‡Mass Spectrometry Facility, Department of Pharmaceutical Chemistry, University of California, San Francisco, California 94158–2517; ¶Laboratory for Molecular Pharmacology, Department of Pharmacology (NPP), UCL, Gower Street, London WC1E 6BT, UK

Received April 26, 2012, and in revised form, August 17, 2012

Published, MCP Papers in Press, October 3, 2012, DOI 10.1074/mcp.M112.019976

[1] The abbreviations used are: AMPA-R, AMPA-type glutamate receptor; Camk2, calcium-calmodulin dependent kinase II; PCC, Pearson correlation coefficient; NMDA-R, NMDA-type glutamate receptors; PSD, postsynaptic density; PSD_{110}, a subset of 110 PSD proteins; SCX, strong cation exchange chromatography.

these proteins at 0, 10, 20, and 60 min after the onset of stimulation.

We observed evidence of the coordinated activation of synaptic protein groups, thereby identifying functional core complexes within the PSD. We demonstrate that adopting a quantitative systems biology approach provides insight allowing for a new level of analysis of synaptic function.

EXPERIMENTAL PROCEDURES

Pharmacological Mass Stimulation—Mice (strain C57BL/6J; male, 3 to 4 months) were injected intraperitoneally with 140 to 150 μl of a 0.05-mg/μl pilocarpine solution in 0.9% NaCl (7 to 7.5 mg/mouse) (10). 2 to 3 min after injection they developed signs of seizures (stage 1 on the Racine scale (11)), which gradually reached stage 4 or 5 within 5 min. Animals were culled 10, 20, and 60 min after pilocarpine injection according to UK Home Office regulations by dislocation of the neck. The forebrain (without olfactory bulbs) was dissected in less than 2 min after culling and flash frozen in liquid nitrogen. All animals that did not show signs of stage 4 or 5 10 min after pilocarpine injection (4 out of 40) were not considered for the experiment and were culled. Control animals (time point 0) were injected with 150 μl of 0.9% NaCl and culled 10 min later, and their brains were acquired as above. Animal experiments were conducted under licenses of the UK Home Office.

PSD Sample Preparation and Quality Control—Three biological replicates of the pilocarpine stimulation were conducted. For each replicate, PSD samples from the four time points were purified in parallel at 4 °C, as outlined elsewhere (9). The material for each time point was obtained from three animals that were pooled prior to the biochemical purification. The brain tissue was homogenized in a sucrose buffer containing a mixture of phosphatase inhibitors (1 mM Na_3VO_4, 1 mM NaF, 1 mM Na_2MoO_4, 4 mM sodium tartrate, 100 nM fenvalerate, 250 nM okadaic acid) and cleared via centrifugation. For each brain region, the ratio of buffer volume to starting brain weight was kept constant (10 ml buffer per gram) to ensure that each PSD preparation was exposed to an equivalent level of inhibitors and buffer. The membranous fraction was layered on a sucrose density and fractionated via centrifugation. Synaptic membranes were collected at the 1.0–1.2 M interface and applied onto a second gradient. The PSD fraction was collected at the 1.4–2.2 M interface and pelleted. During the final pelleting stage, PSD material from a single time point was pelleted into two or more tubes. For each of the three biological replicates, two technical replicates (consisting of one set of tubes) were processed as described below on separate days. The average yield of PSD sample per brain was 0.8 mg. We did not detect alpha-synuclein, a major soluble presynaptic protein (supplemental Tables S1 and S2).

Proteolytic Digestion of PSD Samples—For the four time points in a given replicate, 500 μg of each PSD sample was processed in parallel. Each PSD sample was resuspended in 25 mM ammonium bicarbonate containing 6 M guanidine hydrochloride. The mixture was incubated for one hour at 57 °C with 2 mM Tris(2-carboxyethyl)phosphine hydrochloride to reduce cysteine side chains. These side chains were then alkylated with 4.2 mM iodoacetamide in the dark for 45 min at 21 °C. The mixture was diluted 6-fold with 25 mM ammonium bicarbonate, and 5% (w/w) modified trypsin (Promega, Madison, WI) was added. The pH was adjusted to 8.0, and the mixture was digested for 12 h at 37 °C. The digests were desalted using a C_{18} Sep Pak cartridge (Waters, Milford, MA) and lyophilized to dryness using a SpeedVac concentrator (Thermo Electron, San Jose, CA).

iTRAQ Labeling of Tryptic PSD Digests—The dried peptides were resuspended in 80 μl of iTRAQ dissolution buffer. Each iTRAQ reagent vial was reconstituted using 70 μl of ethanol, and a total of five reagent vials were used to label each 500-μg digest of tryptic peptides. The labeling reaction was allowed to proceed for one hour at 21 °C. An aliquot was then examined using a one-hour LC-MS/MS run and searched allowing iTRAQ as a variable modification to confirm that over 99% of all peptides identified showed complete iTRAQ labeling. A second aliquot containing a 1:1:1:1 mixture of the four labeled samples was then analyzed via LC-MS/MS to determine whether any correction for protein amount needed to be made during the final combination of the four samples.

Strong Cation Exchange Chromatography (SCX)—SCX was performed using an ÄKTA Purifier (GE Healthcare, Piscataway, NJ) equipped with a Tricorn 5/200 column (GE Healthcare, Piscataway, NJ) packed in-house with 5 μm 300 Å polysulfoethyl A resin (Western Analytical, Lake Elsinore, CA). The 2.0 mg combined PSD sample was loaded onto the column in 30% acetonitrile, 5 mM KH_2PO_4, pH 2.7 (buffer A). Buffer B consisted of buffer A with 350 mM KCl. The gradient went from 1% B to 29% B over 19 ml, from 29% B to 75% B over 14 ml, and from 75% B to 100% B over 2.5 ml. Between 90 and 100 fractions were collected and desalted using a MAX-RP reverse phase C_{18} cartridge (Phenomenex, Torrance, CA) and dried down using a SpeedVac concentrator.

Nano-LC-ESI-Qq-TOF Tandem Mass Spectrometry Analysis—Individual SCX fractions were separated using a 75 μm × 15 cm reverse phase C_{18} column (LC Packings, Sunnyvale, CA) at a flow rate of 350 nl/min, running a 3%–32% acetonitrile gradient in 0.1% formic acid on an Eksigent. Gradient cycle times were between 1.0 and 1.5 h in length, depending on sample complexity. The LC eluent was coupled to a micro-ionspray source attached to a QSTAR Pulsar Elite mass spectrometer (Applied Biosystems, Foster City, CA). MS spectra were acquired for 1 s, and the two most intense multiple charged peaks were selected for the generation of subsequent collision-induced dissociation MS. For precursor ion selection, the quadrupole resolution was set to "high," which allows for transmission of ions within approximately ±0.5 *m/z* units of the monoisotopic mass. The collision-induced dissociation energy was automatically adjusted based upon the peptide charge and *m/z* ratio. A dynamic exclusion window was applied that prevented the same *m/z* from being selected for 3 min after its initial acquisition.

Interpretation of MS/MS Spectra—Data were analyzed using Analyst QS software (version 2.0), and MS/MS centroid peak lists were generated using the Mascot.dll script (version 1.6b18). The MS/MS spectra were searched against the entire Uniprot Mus musculus database (downloaded December 2008, with a total of 60,123 entries, to which were appended SHAN1_RAT and SYGP1_RAT). To this database, a randomized version was concatenated to allow for calculations of false discovery rates. Initial peptide tolerances in MS and MS/MS modes were 200 ppm and 0.2 Da, respectively. Trypsin was designated as the protease, and two missed cleavages were allowed. Carbamidomethylation and iTRAQ labeling of lysine residues were searched as fixed modifications. The peptide amino termini were fixed as either iTRAQ modified or protein N-terminal acetylated. Oxidation of methionine was allowed as a variable modification. All high-scoring peptide matches (expectation value < 0.01) from individual LC-MS/MS runs were then used to internally recalibrate MS parent ion *m/z* values within that run. Recalibrated data files were then searched with a peptide tolerance in MS mode of 50 ppm. Peptide hits were considered if they had peptide scores of ≥15 and expectation values of ≤0.05. Across all six analyses, a total of 720,890 MS/MS spectra were acquired, of which 168,513 matched to peptides (including redundant identifications) using the initial acceptance criteria. For the resulting output, UniGene entries were mapped onto the corresponding UniProt accession numbers, and proteins were condensed to single entries if they matched to the same UniGene entry. Peptides that corresponded to proteins from more than one UniGene entry

were not used. UniGene entries were considered identified if they were found with at least two unique peptides.

Across all six analyses (two technical replicates each of the three biological replicates), a total of 3321 unique UniGene entries were identified in at least one of the analyses, and 12 proteins were identified from the decoy database false discovery rate (FDR = 0.4%). A total of 911 Unigenes (and no decoy proteins) were identified with at least two peptides per protein in all six of the analyses.

Quantification of Protein Expression—The raw MS data in *.wiff format were read directly using Protein Prospector (version 4.24.4). For each peptide MS/MS spectrum, the raw area of the peaks at *m/z* 114.1, 115.1, 116.1, and 117.1 (±0.1 *m/z*) was determined. iTRAQ area measurements were adjusted using isotope correction values supplied by the vendor for these batches of the reagent. Only MS/MS spectra in which the most intense iTRAQ peak was ≥25 counts were used. If multiple MS/MS spectra were collected for the same peptide at the same charge state, only the best scoring spectra were used for quantification. To calculate the relative percentage of a given peptide in each of the four samples, the area of that corresponding peak was divided by the average area for all four iTRAQ diagnostic ions in those MS/MS spectra. Relative protein expression values for each UniGene protein entry were the log-averaged value of all peptides matching to that entry.

Following the analysis of the expression ratios between the technical replicates, the 18 proteins (2% of 911) that showed the largest variations between any pair of the technical replicates were considered outliers and were removed, leaving 893 proteins for bioinformatic analysis, for which the two technical replicates for each protein where averaged into one value per time point. This was followed, separately for each biological replicate, by 10 rounds of iterative normalization for each protein, so that the sum of the time points equaled 4, and total protein amount per time point, so that the sum of all proteins equaled 893.

Internal Standard Validation of iTRAQ Quantification—In two sets of biological replicates, four proteins were spiked into the PSD pellets prior to resuspension to estimate the magnitude of iTRAQ compression as a function of the isolation window. Bovine albumin and human transferrin were each spiked in at a 1:2:4:8 ratio. Human hemoglobin and bovine casein were each spiked in at a 1:3:9:27 ratio, allowing a series of 1:2 and 1:3 ratio comparisons. The subset of peptides from these proteins that were identical to mus musculus were excluded from quantification. For those biological replicates with these internal standards, all SCX fractions were analyzed twice using different Q1 isolation settings. The first setting corresponded to the "high" setting on the QSTAR (isolation setting values 0.1 higher than "low"), and the other represented a narrower "custom" isolation (isolation setting value 0.45 higher than "low"). The median observed protein ratio for expected 2- and 3-fold changes were 1.4 and 1.6 using the "high" setting and 1.8 and 1.8 using the "custom" setting. Therefore, all PSD quantification data were acquired using the narrow "custom" setting. Whereas changes in protein expression 3-fold and greater showed substantial compression at these settings, changes 2-fold (and less) were less affected.

Nomenclature of Proteins—For all proteins, we have used the non-italicized version of the gene name as the protein name in all tables and figures. In the text, a protein may additionally be referred to by its common protein name.

Bioinformatic Analysis—Expression profiles and histograms were calculated and displayed in IGOR 6.x. (Wavemetrics, Portland, OR). Pearson correlation coefficients (PCCs) were calculated via the Pearson correlation. Correlation networks were displayed using Cytoscape (version 2.7.0) (12). Details are given in the respective figure legends. Statistical calculations were performed using R (version 2.11.1).

Weighted expression network analysis (13, 14) was conducted to group proteins based upon their temporal patterns using R (version 2.11.1). Custom libraries used for the analysis included dynamicTreeCut, moduleColor, and WGCNA (15) using the following parameters: power = 9; minconnections = 0.01; hclust method = "average"; cutHeight = 0.99, minClusterSiz = 20, method: "tree"; deepSplit = TRUE.

The PSD_{110} Proteins—To reduce the influence of co-purified proteins on the correlation analysis, we defined a subset of 110 proteins (PSD_{110}) representing generally accepted components of PSDs, and we refer to this group as the biochemical core of PSDs. The starting point of this list is the analysis of an affinity-purified PSD preparation (16), which was analyzed by a less deep-reaching MS strategy than we employed here. Our analysis had 97 proteins overlapping with the biochemical PSD core complex from Fernandez et al. (16). We further added the 13 proteins Lrrc7 (Densin-180), Actn1 (Actinin 1), Actn2 (Actinin 2), Ank3 (Ankyrin 3), Camk2d, Cask, Cdh2 (Cadherin 2), Ctnnb1 (Catenin β1), Ctnnd2 (Catenin δ2), Nlgn1 (Neuroligin 1), Shank2, Shank3, and Synpo (Synaptopodin), which (a) were part of the Gene Ontology term "synapse" and generally accepted PSD components (17), (b) were localized neither exclusively presynaptically nor at inhibitory synapses, and (c) had at least 10% sequence coverage in our MS analysis (supplemental Table S1). The PSD_{110} components are listed in supplemental Table S3.

RESULTS

Mass Stimulation of the Central Nervous System Induces Changes in Protein Amounts at Synaptic Sites—In this study, we addressed the question of how pharmacologically induced synaptic activity affects the relative amounts of synaptic proteins in preparations of murine PSDs. We investigated changes occurring during the first 60 min following the onset of stimulation. Changes observed during that period primarily reflect a redistribution of proteins between the purified synaptic compartment and the remaining extrasynaptic cellular volume, plus possibly some induced protein degradation and limited induced synthesis of new proteins, if any.

In order to induce acute massive synaptic stimulation, mice were treated with interperitoneal injection of pilocarpine (10). PSD preparations were obtained for three biological replicates and were each pelleted into multiple identical aliquots. This allowed us to conduct two technical replicates on each biological replicate, for a total of six independently conducted analyses of the synapse. An outline of the workflow is shown in Fig. 1. The two technical replicates provided very similar measurements, consistent with a high degree of accuracy for protein level quantification. For the 893 proteins that passed our stringency criteria (see "Experimental Procedures"), the median difference between protein measurements across technical replicates was 5.1% for individual time point measurements. For subsequent analyses, the mean of each technical replicate pair was used throughout.

To assess the biological reproducibility, we examined a subset of 12 individual key synaptic protein values in detail (supplemental Fig. S1). For the 12 proteins shown, the median coefficient of variation of protein time point values was 3.8%, whereas for the entire dataset this value was 6.6%. For the profiling of individual protein levels, we averaged the three

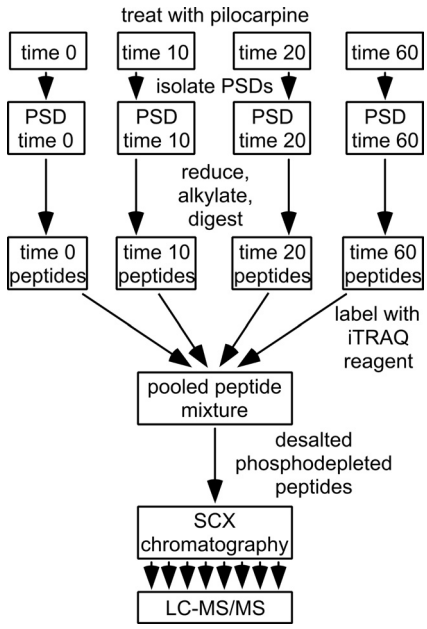

FIG. 1. **Schematic of experimental design and sample processing.** Mice were injected with pilocarpine or sham treated (time 0 min). At 10, 20, or 60 min post-injection, animals were sacrificed and postsynaptic density (PSD) preparations were obtained. Proteins were digested with trypsin, yielding peptides that were then labeled with one of the four versions of the iTRAQ reagent. Labeled peptides were then combined. After depletion of phosphorylated peptides, the sample was fractionated via strong cation exchange (SCX), resulting in 70 fractions. Each of these fractions was analyzed via LC-MS/MS to identify and quantify relative peptide abundances.

biological replicates. For correlation analysis, the time points from each of the three biological replicates were kept as unique datapoints.

Dynamic Localization upon Mass Stimulation Is Consistent within Certain Families of Key Synaptic Proteins—We first determined the overall changes in protein levels. 95% of all changes are within a ±15% range (Fig. 2*A*). The variations within the biochemical core proteins (PSD_{110}; see "Experimental Procedures" and below) were of comparable magnitude (Fig. 2*C*). Ratios between the minimum and maximum levels of individual proteins had a median of 1.115 (Fig. 2*B*). Taken together, massive synaptic stimulation induced relatively modest overall changes in protein levels within the complete population of forebrain synapses.

We next analyzed members of protein families that shared a high degree of sequence similarity. The subunits of AMPA-Rs (18), which are the main determinants of synaptic strength, were strikingly correlated in the response to mass stimulation. In particular, Gria1, Gria2, and Gria3 (GluA1, GluA2, and GluA3, respectively) displayed nearly identical dynamics (Fig. 2*D*).

NMDA-Rs (19) are the primary mediators of coincident neuronal stimulation and are involved in input pattern recognition. It is clear that levels of Grin1, Grin2a, and Grin2b (GluN1, GluN2A, and GluN2B) protein behave nearly identically, with Grin2d (GluN2D) showing less correlation (Fig. 2*E*). Both NMDA-R and AMPA-R subunits showed a profile of about ±10% change, with an initial increase peaking at 20 min and a return to near-baseline values after 60 min.

Within the Dlg family (20) of adaptor proteins, Dlg4 (PSD95) and Dlg2 (PSD93/Chapsyn110) show very similar patterns, with maximum synaptic localization at 20 min. In contrast, the average levels of Dlg1 (SAP97) protein are minimally changed in response to stimulation (Fig. 2*F*).

A markedly distinctive pattern was observed for all four isoforms of calcium-calmodulin dependent kinase II (Camk2) (21), a major kinase involved in synaptic plasticity, which showed a sustained decrease across the time-course of the experiment (Fig. 2*G*). Sixty minutes post-pilocarpine injection, there was a 10% to 20% decrease in the average Camk2 content at the synapse.

The AP2 components of the adaptor protein complex 2 (22) were strongly co-regulated with a small increase in synaptic protein levels during the time course of the experiment (Fig. 2*H*).

A group of filament-forming GTPases, the septins, are necessary for organization of the actin cytoskeleton and localize to the neck of synaptic spines (23, 24). They display concerted regulation in synaptic protein levels with a minimum at 20 min after stimulation (Fig. 2*I*).

In these examples, members of gene families often, but not always, show a coordinated pattern. Direct interaction within some members of a gene family are expected and well established, such as for AMPA-R subunits, which co-assemble into heterooligomeric receptors (18). Further, components of the adaptor protein complex (AP2) show tight correlation in line with co-assembly of the components (22). The DLG family members Dlg2 (PSD93/Chapsyn110) and Dlg4 (PSD95) showed coordinated regulation, whereas Dlg1 (SAP97) does not follow their expression pattern. This suggests that the relative synaptic levels of Dlg2 and Dlg4 are being either dominated by co-assembly or, in the absence of co-assembly, co-regulated by a concerted process. In the latter case, it is likely that cis-regulatory domains must have been conserved between Dlg2 and Dlg4 but not with Dlg1.

Dlg4 (PSD95) is Highly Positively Correlated with Core Synaptic Proteins—To investigate coordinated regulation over the full set of 893 proteins, we calculated all pair-wise PCCs using all 12 time point values per protein. The distribution histogram had a median of essentially 0 (PCC = 0.012) (Fig. 3*A*), indicating no correlation. The top 5% of positive correlations had PCCs > 0.7034. The mirror threshold PCCs < -0.7034 defined a group only 3.5%, indicating a preference for strongly positive correlated changes in protein amounts. To test whether this large-scale examination of correlation revealed information about biological function, we investigated the key postsynaptic synaptic protein Dlg4 (20) in detail. Whereas the median Dlg4 correlation with all other 892 proteins was shifted

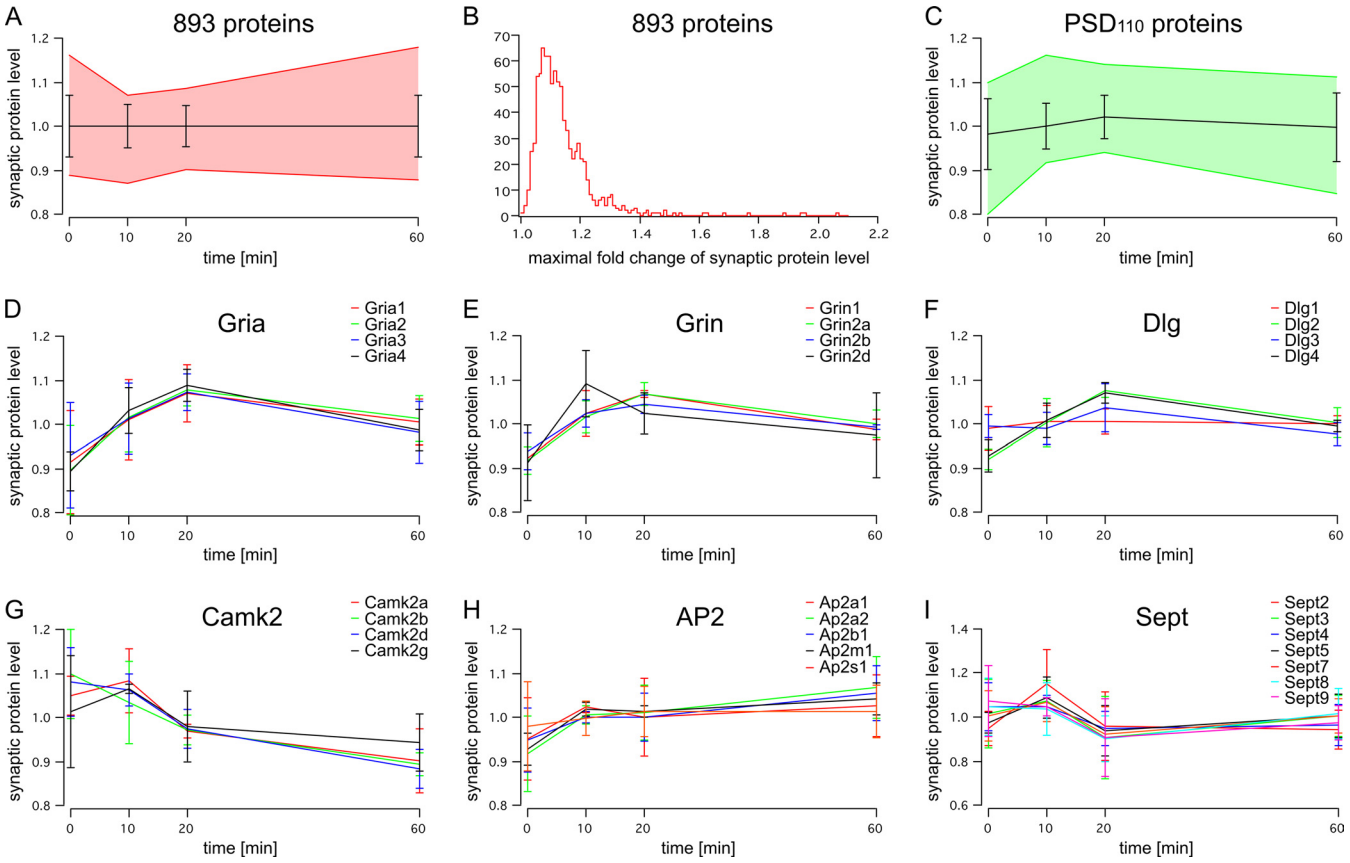

FIG. 2. **Comparison of synaptic localization dynamics for selected proteins.** The range of synaptic protein levels is shown for all 893 identified proteins (*A*) and for the PSD_{110} proteins (*C*) with mean ± S.D. and 95% of all values within the colored area. *B*, histogram of the maximal change in the synaptic protein level for each of the 893 proteins. *D–I*, dynamic profile for selected protein families. For each of the three biological replicates, the data were combined to give an average profile for each protein. Error bars represent the standard error of the mean for each of the three replicates. All four AMPA receptors display correlated changes with a maximal localization at 20 min (*D*). NMDA-type glutamate receptors display similar correlated changes (particularly for Grin1, Grin2a, and Grin2b) as shown in *E*. For the Dlg family of scaffolding proteins, Dlg2 and Dlg4 show patterns similar to each other and to that of NMDA receptors (*F*). The Camk2 isoforms show a sustained decrease throughout the experiment, with a minimum at 60 min. It is known that alpha Camk2 can originate from local translation. The overall declining pattern supports the notion that we observed translocation, and not new protein synthesis (*G*). Most components of the AP2 complex (*H*) and the members of the septins display a correlated dynamic profile (*I*).

slightly to more positive values (median PPC = 0.077; Fig. 3*B*), the percentage of highest correlating (*i.e.* PCC > 0.7034) pairs was increased (6.4%). This shift was even stronger in the subset of correlations of Dlg4 with the other 109 PSD_{110} proteins (see "Experimental Procedures" and supplemental Table S3), with a median PCC = 0.401 and with 17% of PCCs > 0.7034 (Fig. 3*C*), confirming their tight correlation in localization dynamics. We then compared our data to published protein interactions. The IntAct database listed 46 proteins that have been experimentally demonstrated to interact with Dlg4 (supplemental Fig. S2*A*) (38); 22 of these proteins were identified in our postsynaptic preparation, of which 20 were also part of the PSD_{110} complex (Fig. 3*D*, supplemental Fig S2*B*). The median PCC between Dlg4 and these 22 proteins (0.374) is very similar to the median value observed between Dlg4 and the 109 other PSD_{110} core proteins. As an example, the dynamic profile of Dlg4 is shown (Fig. 3*E*) together with the strongest correlating dynamic profiles of directly interacting proteins (green in supplemental Fig. S2).

Taken together, these analyses demonstrate that the relative quantitation we performed is well suited to reveal activity-dependent co-regulation of proteins despite the relatively small changes in protein abundance that were observed. It further suggests that within the group of PSD_{110} proteins, Dlg4 might be highly connected.

Correlation Network of the PSD_{110} Proteins Implies an Interconnected Core of Co-regulated Postsynaptic Proteins—We next asked the question of which close interactions exist between proteins of a biochemical PSD protein complex that is derived from a more stringent purification procedure and limited to the more abundant proteins (16, 17, 25). Within the PSD_{110}, we investigated the extent to which individual protein levels were co-coordinately regulated. Overall, we observed that individual members displayed a higher de-

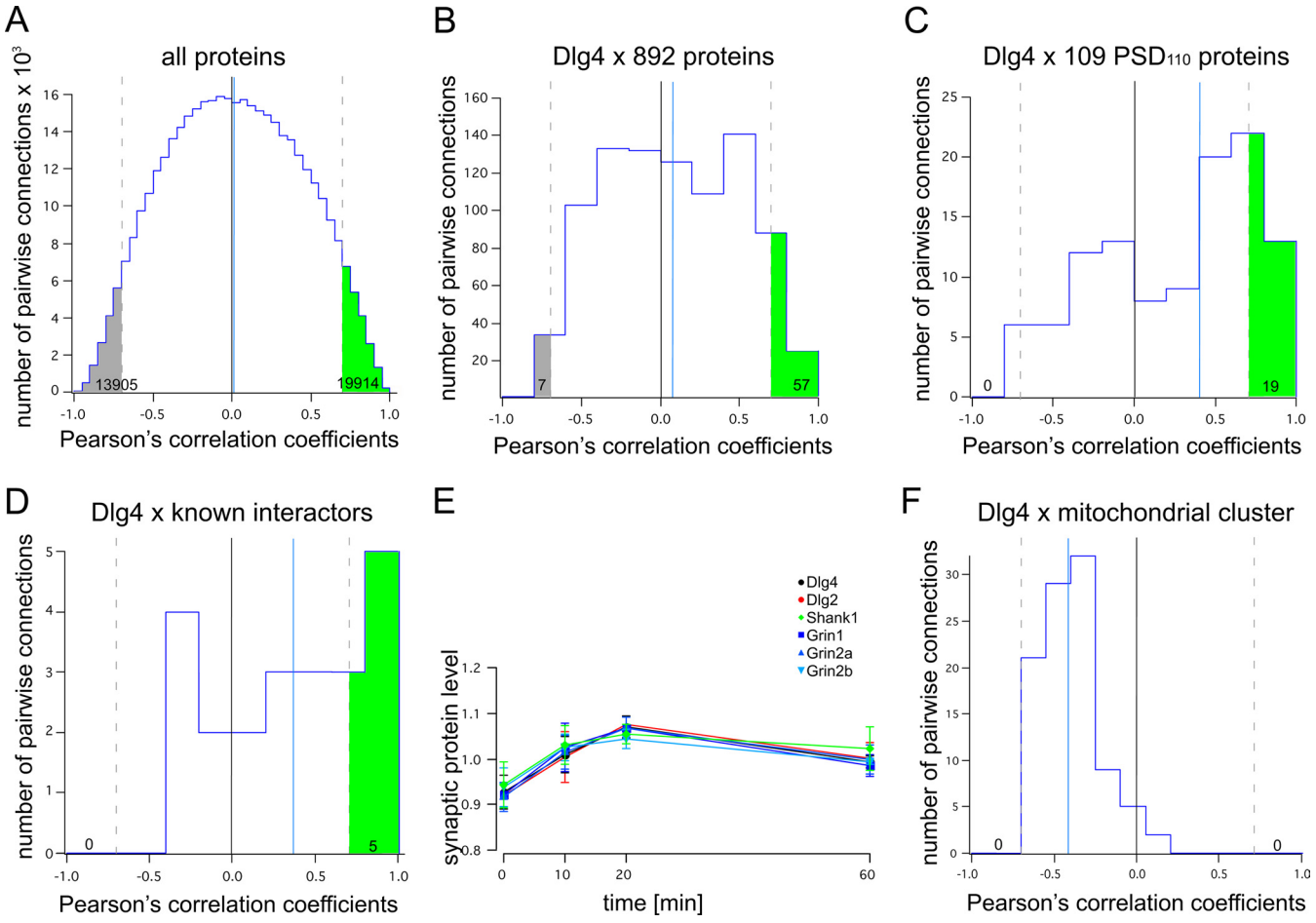

FIG. 3. **Histogram of non-redundant pairwise Pearson's correlation coefficients (PCCs).** *A*, PCCs within entire dataset of 893 proteins (total: 398,278). *B*, PCCs of Dlg4 with all 892 proteins (total = 892). *C*, PCCs of Dlg4 with PSD core complex proteins (total: 109). The highest correlating pairs (green) with PPC > 0.7034 correspond to 5% (*A*), 6.4% (*B*), and 17% (*C*), and the pairs with PCC < −0.7034 (gray) correspond to 3.5% (*A*), 0.8% (*B*), and 0% (*C*) of all correlation pairs. Data are skewed, with the median (orange line) shifting to 0.012 (*A*), 0.077 (*B*), and 0.401 (*C*). *D*, histogram of PCCs of 22 identified proteins that are known interaction partners of Dlg4 (IntAct; total: 46 proteins). 20 of 22 identified interaction partners are also part of the PSD_{110} complex (supplemental Fig. S2). Median: 0.374. Five proteins correlate with Dlg4 with a PPC > 0.7034 (green bars; 23%). The stimulation profiles of these five are shown together with the one for Dlg4 (*E*). *F*, histogram of PCCs of Dlg4 with the 99 proteins in the mitochondrial complex defined in Fig. 5*B* (cluster II). There is a strong shift to negative correlations with a median PCC = −0.420.

gree of correlated dynamics relative to the entire dataset. If we examined those PCC values corresponding to the top 1.0% for the entire dataset (PCC > 0.853), PCC values between pairs of PSD_{110} proteins were 2.5-fold enriched relative to the entire dataset ($p < 1.99\times 10^{-24}$, hypergeometric distribution).

A PCC of >0.7034 segregates the top 5% all correlations (Fig. 3*A*, 19,913 out of 398,278). 99 of the PSD_{110} proteins were correlated with at least one other PSD_{110} protein above this threshold, defining a total of 582 connections (supplemental Table S4), which are indicated as edges in Fig. 4. 27 proteins accounted for more than 50% of all such connections. Included in the highly connected subset are Dlg4, Grin1/2a/2b, and Lrrc7. These proteins were among the earliest identified PSD components, and the Dlg4-Grin2 PDZ domain-mediated interaction was one of the initially reported strong and reversible interactions of postsynaptic proteins (25, 26).

Closer inspection revealed that this group of 27 proteins contained all widely expressed AMPA-R (three) and NMDA-R subunits (four), plus two co-assembling Kainate-type glutamate receptor subunits (Grik2/GluK2 and Grik5/GluK5). In addition, nine adaptor and scaffolding proteins were found as the highest connected nodes (highlighted in Fig. 4). Given that these adaptor and scaffolding molecules interact with multiple other synaptic proteins, this suggests that the core 27 protein cluster might regulate a larger subset of synaptic proteins following mass stimulation.

Regulation of the PSD_{110} Proteins with Respect to a Larger Dataset—We next asked the question of how robust our identification of the above-identified co-regulated functional

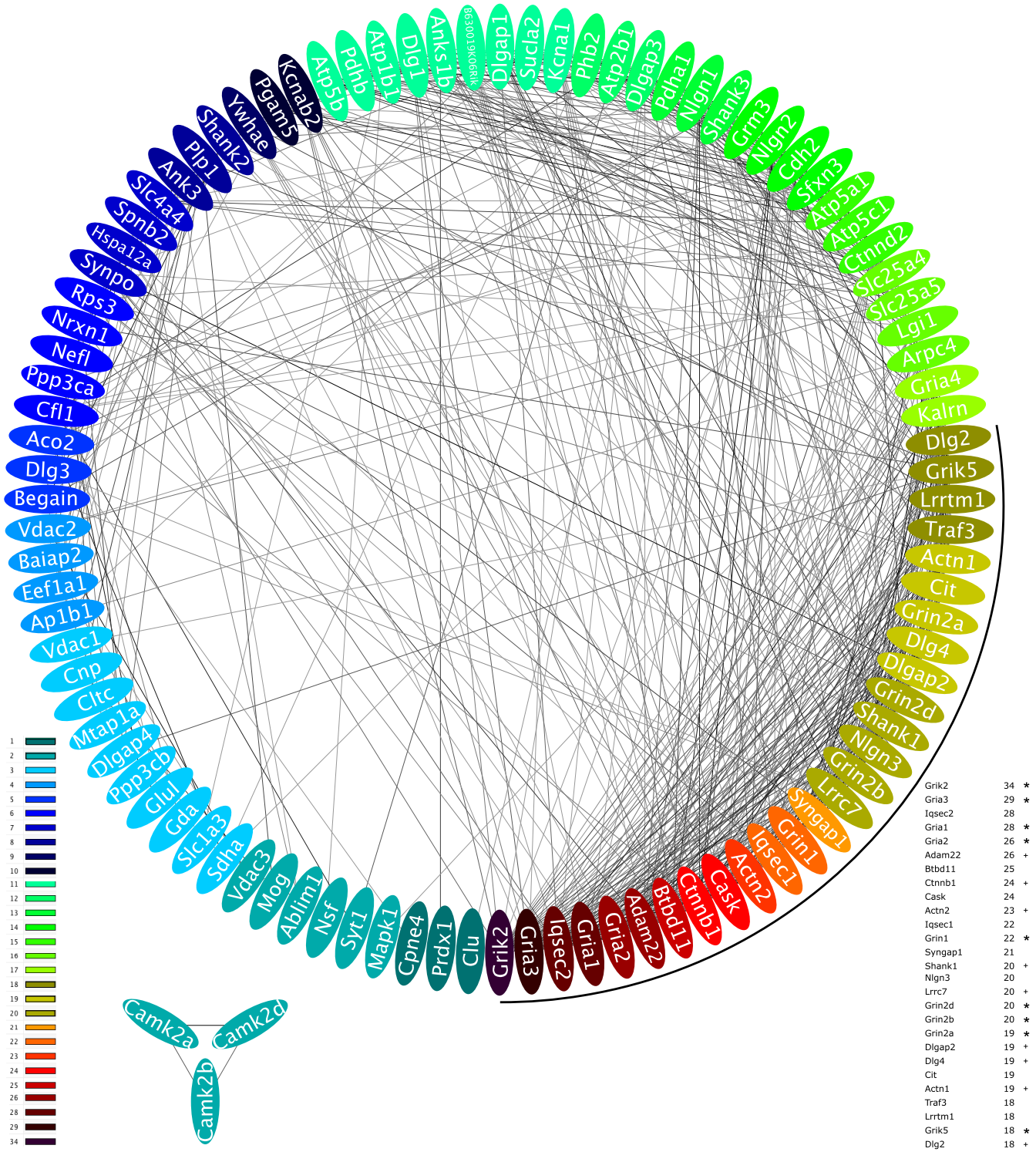

FIG. 4. **Correlation network of identified proteins belonging to the PSD$_{110}$ complex.** Degree sorted circle representation. Nodes represent individual proteins, and edges represent correlations within a cutoff corresponding to the top 5% of all pairwise correlations (PCC > 0.7034) within the entire dataset of 893 proteins (listed in supplemental Table S4). Lines are shown graded by strength of correlation ranging from light gray (PCC = 0.7034) to black (PCC = 1.0000). Nodes are colored according to the number of connections above PCC > 0.7034. The 27 highest connected proteins amounting for >50% of all connections are highlighted (black circle segment) and listed with the number of connections. Members of the glutamate receptor family are highlighted (*), as are adaptor/scaffolding proteins (+).

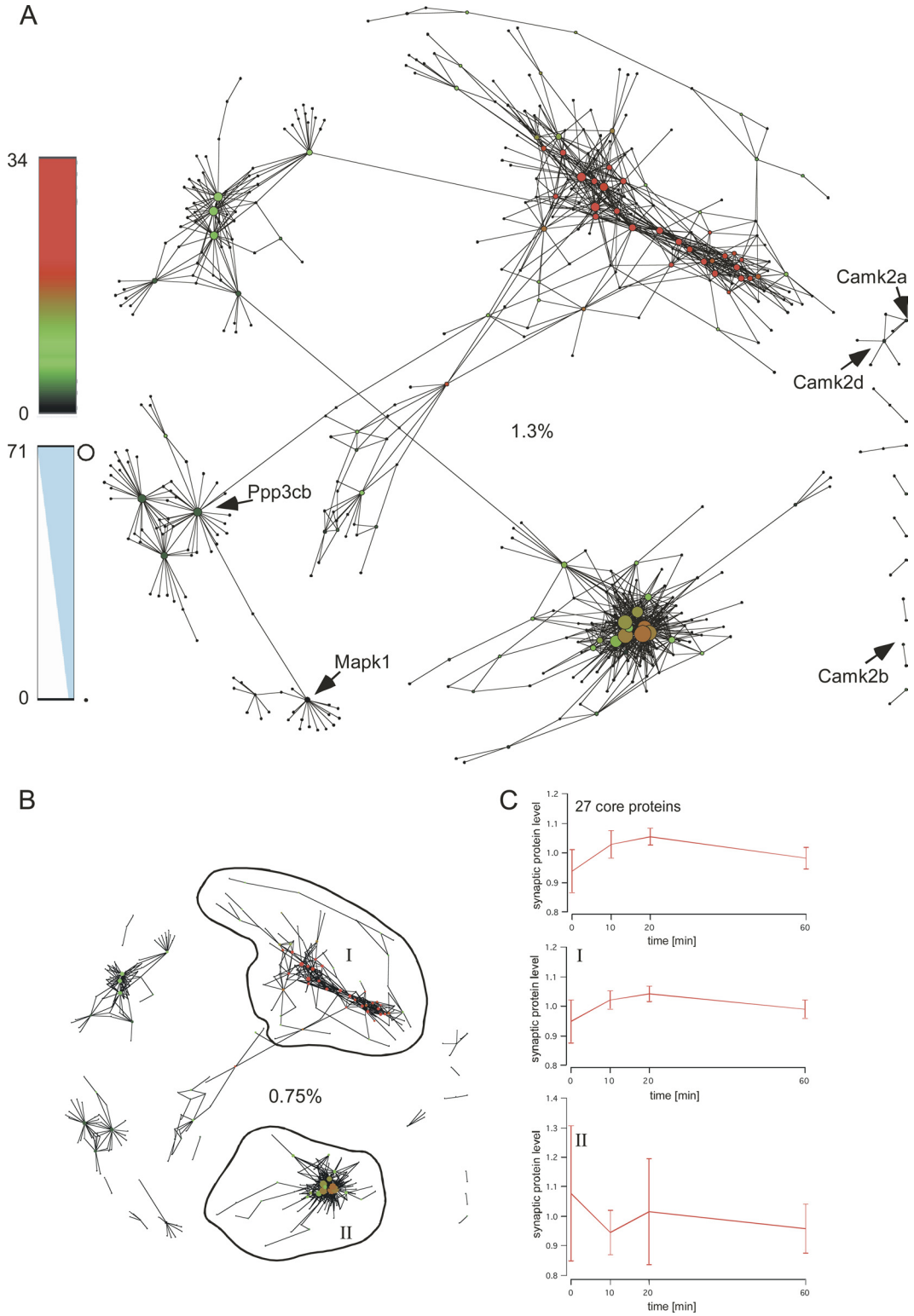

FIG. 5. **Correlation network of PSD_{110} protein and near neighbors.** PCC correlations displayed as spring-embedded, force-directed, and unweighted networks. *A*, the best 1.3% (PCC > 0.83625) of correlation pairs are depicted (see supplemental Table S5). *B*, the best 0.75% (PCC > 0.86972). The degree of connectivity of PSD_{110}–PSD_{110} connections is color-coded (number of connections from Fig. 4). PSD_{110} proteins (size graded by degree of connectivity) seem to often be a hub for a multitude of non-PSD_{110} proteins (black). Two clusters are defined (I, II) that are stable when raising the threshold of the PCC from *A* to *B*. These clusters contain 136 and 99 proteins, of which 38 and 21% are PSD_{110} proteins, respectively. Members of clusters I and II are listed in supplemental Table S6. Functional annotation of proteins in clusters:

core is when we include proteins beyond the PSD_{110} dataset. We therefore extended the analysis to PCC of protein pairs with at least one component from the PSD_{110} dataset, and the other not necessarily a PSD_{110} member, which we call here near neighbor proteins. Under the assumption that protein pairs showing highly correlated stimulation-dependent dynamics are more likely to directly interact, we looked at the best 1% pairwise correlations (Fig. 5*A*).

Correlations depicted in this network are all of very similar values ($0.83625 < PPC < 0.99727$). Nevertheless, a spring-embedded layout, which groups together subsets of proteins with a high degree of interconnection, suggested two major clusters. These two clusters are mainly formed by the highest correlated protein pairs, and raising the threshold to >0.86972 kept them essentially intact (clusters I and II) but removed the connections linking them (Fig. 5*B*).

38% of the proteins in cluster I and 21% of the proteins in cluster II were PSD_{110} proteins. Functional annotation of the proteins within the clusters with DAVID (27, 28) revealed a 72-fold enrichment for the Gene Ontology (GO) term "ionic glutamate receptor cluster" for cluster I (after Bonferroni correction, $p < 1.4 \times 10^{-11}$) and a 6.7-fold enrichment for the GO term "mitochondrion" (after Bonferroni correction, $p < 6.4 \times 10^{-42}$). Interestingly, the "glutamate receptor/adaptor" cluster (cluster I) contained 27 out of the 27 core proteins from Fig. 4 and was found to be highly correlated (and thus connected) within the PSD core proteins (as indicated by the red color).

Other PSD_{110} proteins, such as kinases and phosphatases, show many connections to other proteins (Ppp3cb/Calcineurin A beta subunit: 24 connections; Mapk1: 11 connections). Camk2 subunits form a separate minicluster within the PSD_{110} proteins (Fig. 4) and show few strong connections when the near neighbors are included (Fig. 5*A*).

In all, extending the analysis beyond the set of PSD_{110} proteins to their near neighbors returned a cluster of functionally connected proteins (cluster I, Fig. 5*B*) around the originally identified glutamate receptor/adaptor protein group (Fig. 4). This confirms the core position of these groups of proteins in the activity-dependent regulation of synaptic proteins.

In addition, the extended analysis revealed a tightly co-regulated group of proteins (cluster II) connected to mitochondrial proteins. This cluster contained a smaller fraction of PSD_{110} proteins than cluster I and had a higher degree of interconnectivity (6.6 *versus* 4.3 connections per node, respectively).

Robustness of Core Clusters within the Complete Dataset—To test how robust the definition of the functional core complex was with respect to a different method of analysis, we applied weighted expression network analysis of synaptic protein levels to our full dataset of 893 proteins.

The clustering dendrogram for the 893 proteins in our dataset is shown in Fig. 6*A*. To partition the dendrogram into clusters, we applied the Dynamic Tree Cut algorithm, which detects clusters based upon the shape of the dendrogram rather than merely utilizing a constant-height branch cut. This resulted in portioning the proteins into 24 clusters plus 106 unassigned proteins (Fig. 6*B*, supplemental Table S6). Each member of the PSD_{110} protein dataset is represented with a green tick mark above the cluster colorbar in Fig. 6*B*. These 110 proteins are widely, but not uniformly, distributed across the dendrogram, indicating that the majority of proteins not in the PSD_{110} protein subset nevertheless are dynamically regulated in a pattern that correlates well with several PSD_{110} proteins. For those 27 proteins most highly connected in Fig. 4, tick marks are colored blue. 18 of these 27 proteins map to a set of three small adjacent clusters (gray, dark turquoise, and green-yellow), and an additional 7 proteins cluster tightly within the turquoise cluster (Fig. 6*B*), consistent with the notion that these proteins constitute a central functional core of the synapse. Notably, these segments (designated alpha and beta) are well separated from the segments to which the vast majority of mitochondrial-associated proteins belong (black tick marks).

Fig. 6*C* shows a topological overlap matrix plot in heatmap representation. The projection of the two segments in the dendrogram (alpha and beta) covering the majority of the 27 core clusters onto the heatmap not only revealed the high correlation within one area, but also indicated a relatively high correlation between the two segments (mean PCC for alpha-beta connections: 0.2011; mean PCC for alpha-alpha correlations: 0.2082; mean PCC for beta-beta correlations: 0.1426), despite that fact that the constraints of mapping all correlations along a one-dimensional hierarchical dendrogram did not place alpha and beta adjacent to each other.

The alpha and beta segments are shown in more detail in Fig. 6*D*. The alpha segment contains the key glutamate receptors Grin1, Grin2a, Grin2b, Gria1, Gria2, Gria3, and Gria4. In addition, this segment also contains the structural/scaffolding molecules Shank1, Lrrc7, Dlgap1, Dlgap2, Dlg2, and Dlg4. Other proteins found in this segment include a number of ion channels (Cacna1a, Cacnb4, Gabbr1, and Ttyh1).

While CaMKII subunits displayed dynamics distinct from this cluster, kinases included here are Kalrn, Cask, and Cit. Finally, these segments included several proteins involved in membrane trafficking and reorganization of the actin cytoskeleton, including Ablim3, Cask, Ctnna2, Fnbp1l, Ppp1r9a, Shank1, Syngap1, and Synpo. The absolute abundance of these proteins (as roughly indicated by peptide count) varies substantially. For example, on average, 57.3 peptides were

(I) 72 enrichment score for the GO term "ionic glutamate receptor complex" ($p_{Bonferroni} < 1.4 \times 10^{-11}$); (II) 6.7 for GO term "mitochondrion" ($p_{Bonferroni} < 6.4 \times 10^{-42}$) (27, 28). Average stimulation profiles for each of the clusters are shown in *C*. Mean ± S.D. All 27 core proteins (from Fig. 4) are within cluster I. Their combined profile is very similar to the cluster I profile.

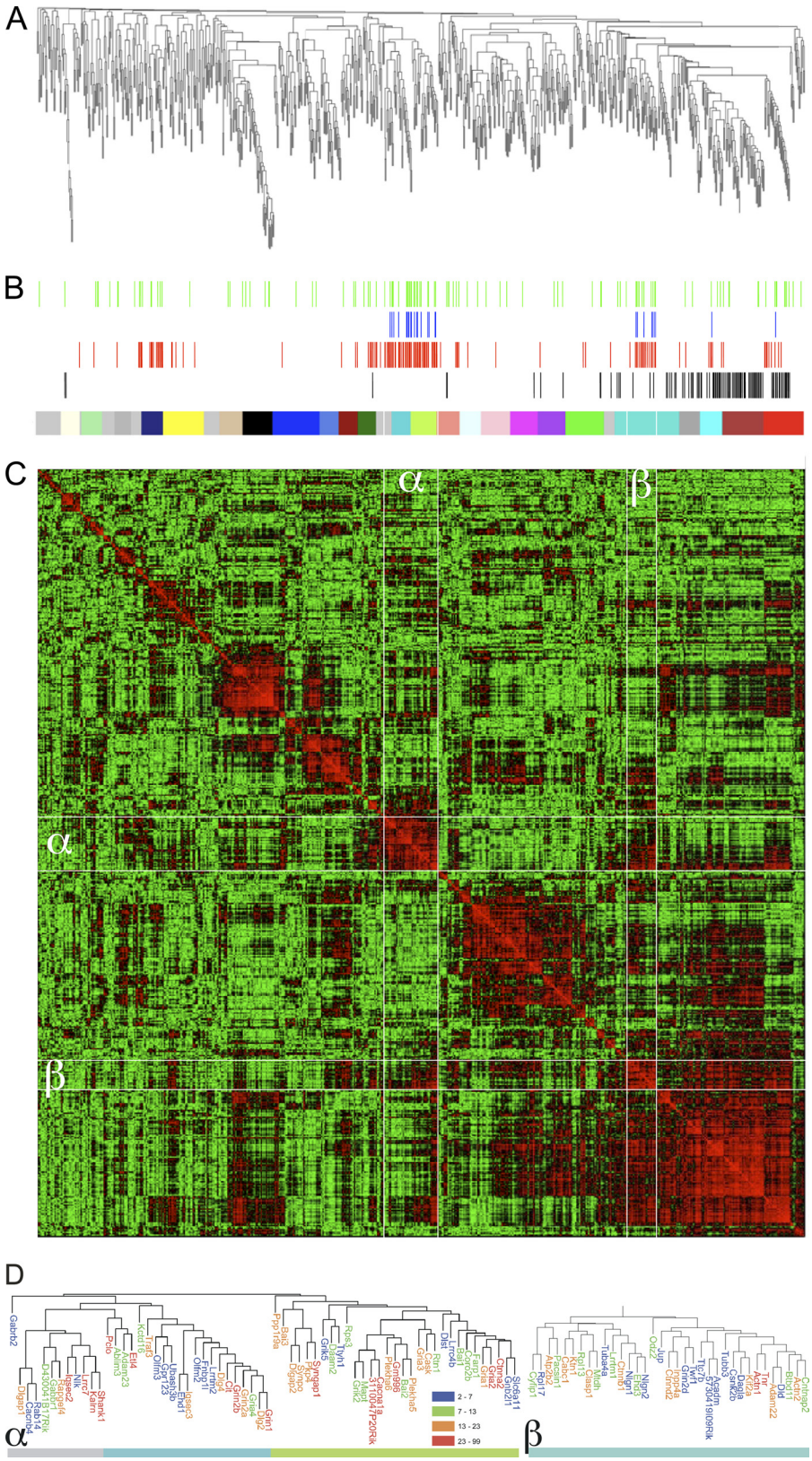

FIG. 6. **Weighted expression network analysis of the entire PSD dataset.** *A*, weighted expression network analysis was performed to yield the dendrogram. *B*, to group proteins within the dendrogram, the program Dynamic Tree Cut was applied, resulting in 24 clusters plus 106 proteins not assigned to a distinct cluster (gray). Hashmarks above the clusters represent the location within the dendrogram of the PSD_{110}

found for Syngap1, whereas 6.5 peptides were found for Grik5.

Taken together, our results demonstrated that synaptic composition is highly regulated by activity. We identified two distinct clusters whose proteins showed highly coordinated stimulation-dependent regulation. The first cluster is dominated by ionotropic glutamate receptor subunits and adaptor proteins, and the second by mitochondria-associated proteins.

DISCUSSION

Synapses are dynamic subcellular compartments with protein compositions that are regulated by a large number of interconnected pathways in an activity-dependent fashion. Here we sought to identify functional core clusters representing the most co-regulated groups of synaptic proteins following synaptic stimulation, independent of whether the individual members are governed by direct physical interaction. We have chosen to use a chemical mass-stimulation protocol that relies on intraperitoneal injection of the muscarinic acetylcholine agonist pilocarpine. This is a well-established model for acute seizure induction, which we take here as an expression of high synaptic activity during the 60 min duration of the experiment.

Biological Relevance of Observed Dynamic Profiles—We observed relatively modest changes in protein levels, even for proteins such as Gria1 and Camk2, which have been reported to undergo large changes in localization in response to activity. Several possibilities exist for reconciling these observations. Firstly, our stimulation protocol might not have activated all synapses, and therefore the magnitude of changes at the most regulated synapses might have been diluted. Secondly, our preparation contains a heterogeneous population of synapses that might not be equally affected by stimulation (in either magnitude or kinetics). The latter dilution effect could be overcome with the investigation of synapses from smaller brain regions or specific neuronal cell populations once more sensitive robust quantitation strategies can be employed. Lastly, iTRAQ quantitation of complex samples is prone to range compression (39) and is not suitable for precisely measuring large ratios in complex samples. However, measurements of spiked internal protein standards demonstrate that iTRAQ range compression is mild at the fold-changes we observed using our specific mass spectrometric acquisition parameters (see"Experimental Procedures").

In principle, the changes in synaptic composition we detected might result from redistribution into/out of extrasynaptic regions and/or protein synthesis/turnover. Dendritic protein synthesis is well characterized in several instances (29), although this is limited to a small subset of synaptic proteins and thus will not explain the majority of our observations. Protein degradation is unlikely to be directly responsible for decreases in protein levels. We did not detect substantial increases in ubiquitin, and given that proteosomes are not enriched at the synapse, targeted degradation would be secondary to translocation out of synaptic compartments. Upon sacrifice, mouse cortexes were immediately dissected and frozen in liquid nitrogen. Nevertheless, we cannot rule out the possibility that some of the changes we observe occurred peri- or post-mortem.

Despite changes only on the order of $\pm$15%, the very similar expression profiles observed for co-assembling members of gene families substantiated the validity of our measurements.

Our analysis, however, does not have the resolution to address mixed populations of co-assembled subunits. One example of this is that the precise subunit composition of AMPA-Rs can vary from synapse to synapse. Another example is the Grin2d subunit, whose limited presence in a small fraction of NMDA-Rs (19) and restriction to a small subset number of neurons can easily explain its more deviant behavior with respect to other members of the Grin family, even if their overall patterns are similar.

The analysis of protein profiles within selected gene families revealed a conserved profile for most members. This can be partially explained by their physical co-assembly, but it also might indicate that protein domains governing activity-dependent subcellular distribution have been maintained during the evolution of the individual family. The most obvious exception is Dlg1/Sap97, for which we did not observe activity-dependent redistribution. A similar flat Dlg1 profile has been observed for different stimulation protocols in primary neuronal cultures at comparable time points (31).

Definition of Functional Core Clusters within PSDs—Dlg4 is one of the more abundant proteins in PSD preparations. It constitutes about 1% of the PSD protein content and has multiple known protein–protein interactions (17). In our dataset, Dlg4 showed a strong positive correlation with most of its known interaction partners, indicating that our dataset is well suited for a more detailed analysis of co-regulated protein behavior.

One shortcoming with many types of bioinformatic analysis of co-regulation lies in the fact that *a priori* each protein is given equal weight. In particular, the absolute abundance of proteins might differ by 3 orders of magnitude or more within

proteins (green), the 27 most highly connected core PSD proteins as determined in Fig. 4 (blue), cluster I from Fig. 5 representing (red), and the mitochondria-associated cluster II (black). *C*, a topographical overlap matrix plot of the dataset. A high degree of similarity is represented in red. Low similarity is represented in green. The α and β segments enclose the branches containing the two groups of blue hashmarks. *D*, a more detailed representation of the α and β segments. Protein abundance as measured by peptide count is indicated by the color of the protein name.

the PSD. Yet absolute abundance data are not available for most PSD components. The analysis is further complicated by the possibility that certain components of the preparation might be partial contaminants due to imperfect initial separation or secondary association during the purification procedure. We therefore analyzed co-regulation initially on a restricted subset of proteins that are generally accepted as genuine PSD components, the PSD_{110} proteins. This analysis suggested a group of 27 highly co-regulated proteins, containing nine ionotropic glutamate receptor subunits and nine adaptor proteins. The composition of this cluster implies that it will directly affect synaptic strength and size (32).

When the analysis was expanded to allow one member of the interaction to not belong to the PSD_{110} set of proteins, the original cluster of 27 proteins still grouped together. This is an important observation, as it supports the centrality of this group of proteins and the robustness of this grouping when the scope of the analysis is expanded.

Noteworthy, in our experiments, NMDA-R and AMPA-R subunits were found to have similar dynamic responses (compare the patterns in Figs. 2*C* and 2*D*). This is in contrast to observations made in certain electrophysiological experiments at individual synapses that have shown independent regulation of AMAP-R and NMDA-R activity (33). Our measurements differ from these recordings in that (i) we measure all PSD-associated subunits and not only surface receptors, and (ii) our measurements reflect a bulk behavior of the entire pool of synapses, whereas electrophysiological measurements emphasize the behavior of single or few synapses. Therefore, our data suggest that despite independent regulation of AMPA-Rs *versus* NMDA-RS at the level of individual synapses, there is an overarching co-regulation at the level of the whole brain.

Synaptic activity has been reported to induce the relocation of Camk2 into spines and, by implication, into PSDs. Our data suggest a minor increase of Camk2a, the dominant Camk subunit, at 10 min and a global decrease over the course of the experiments. Previous studies have indicated a fast reversibility of Camk2 translocation, indicating a low-affinity interaction with the PSD, which is also dependent on the phosphorylation status of Camk2 subunits (34–36). Our data showed surprisingly limited correlated co-regulation of Camk2 within the PSD_{110} group of proteins. The same limited co-regulation was observed with respect to proteins in the extended dataset. Our data are fully compatible with models of multiple low-affinity interactions of Camk2 with PSD components, which might obscure any predominant co-regulated behavior. Any further-reaching interpretation of Camk2 behavior would require quantitative information about the phosphorylation status of the Camk2 subunits.

The second tightly co-regulated cluster contains mainly mitochondria-associated proteins. This cluster is also present in the extended datasets, where its membership increases considerably, as most mitochondria-associated proteins are not considered biochemical core components of PSDs. Being part of an established organelle, their clustering is not surprising. The spatial distribution of dendritic mitochondria is known to be activity dependent (37); however, the precise relationship to the PSD remained unclear. Our data suggest that massive synaptic stimulation leads to a slight decrease in mitochondrial proteins within 60 min. Noticeable is the strong negative correlation between Dlg4 (Fig. 3*F*), the signature molecule of cluster I, and the mitochondrial cluster. We are studying relative protein levels, so if a subset of proteins increases or decreases, then by definition the remaining proteins will appear to be regulated even if their levels are unchanged. Our data indicated a compensatory balance between the relative amounts of the glutamate receptor/adaptor protein cluster I and the mitochondria associated protein cluster II (Fig. 5*C*, supplemental Fig. S3).

CONCLUSIONS

The major focus of large-scale neuronal quantitative studies to date has been on the genome and the transcriptome. Here we present a large-scale quantitative approach for assessing levels of the full postsynaptic proteome targeting a functionally highly specialized subcellular compartment following massive synaptic stimulation.

This led us to identify two functional clusters of strongly co-regulated proteins *in vivo*. One cluster is related to mitochondria and contains a smaller number of major synaptic proteins.

Our major insight consists of the delineation of a second, tightly co-regulated cluster of proteins, composed of mainly glutamate receptors, their adaptors, and closely associated proteins. We propose that this cluster is a functional core of the postsynaptic machinery, and to our knowledge this is the first delineation of a group of activity-dependent co-regulated proteins within the PSD. Because it contains the ensemble of subunits of ionotropic glutamate receptors and the predominant postsynaptic scaffolding and adaptor proteins, changes in its abundance will affect synaptic strength and size.

These results demonstrate the potential of our quantitative approach as a model for future quantitative studies of PSD composition. Changes in synaptic levels of one or a few proteins can influence synaptic function by changing the optimal settings of the synaptic signaling network (8), likely by influencing the otherwise coordinated behavior of co-regulated clusters. Therefore, it will be of future interest to apply quantitative proteomic approaches combined with bioinformatic analysis to address dynamic synaptic protein levels and their interconnected regulation in genetic mouse models of neuropsychiatric diseases.

Acknowledgments—A.B., A.T., J.T., and R.S. planned experiments, analyzed data, and wrote the manuscript. A.T., J.T., and R.S. performed experiments.

* This work was supported by the Wellcome Trust, the Biotechnology and Biological Sciences Research Council (to R.S.), and National Institute of General Medical Sciences Biomedical Research Technology Program Grant No. 8P41GM103481 (to A.L.B.). J.C.T. acknowledges support from NIGMS Center Grant No. P50 GM081879 (to A.L.B., Co-PI).

[S] This article contains supplemental material.

‖ To whom correspondence should be addressed: A. L. Burlingame, E-mail: alb@cgl.ucsf.edu; R. Schoepfer, e-mail: publications@schoepferlab.org.

§ These authors contributed equally to this work.

REFERENCES

1. Sheng, M., and Kim, M. J. (2002) Postsynaptic signaling and plasticity mechanisms. *Science.* **298,** 776–780
2. Henley, J. M., Barker, E. A., and Glebov, O. O. (2011) Routes, destinations and delays: recent advances in AMPA receptor trafficking. *Trends Neurosci*. **34,** 258–268
3. Schulman, H. (2004) Activity-dependent regulation of calcium/calmodulin-dependent protein kinase II localization. *J. Neurosci.* **24,** 8399–8403
4. Perez-Otano, I., and Ehlers, M. D. (2005) Homeostatic plasticity and NMDA receptor trafficking. *Trends Neurosci.* **28,** 229–238
5. Haas, K. F., and Broadie, K. (2008) Roles of ubiquitination at the synapse. *Biochim. Biophys. Acta.* **1779,** 495–506
6. Chang, R. C., Yu, M. S., and Lai, C. S. (2006) Significance of molecular signaling for protein translation control in neurodegenerative diseases. *Neurosignals.* **15,** 249–258
7. Ronesi, J. A., and Huber, K. M. (2008) Metabotropic glutamate receptors and fragile x mental retardation protein: partners in translational regulation at the synapse. *Sci. Signal*. **1,** 6
8. Ramocki, M. B., and Zoghbi, H. Y. (2008) Failure of neuronal homeostasis results in common neuropsychiatric phenotypes. *Nature.* **455,** 912–918
9. Trinidad, J. C., Thalhammer, A., Specht, C. G., Lynn, A. J., Baker, P. R., Schoepfer, R., and Burlingame, A. L. (2008) Quantitative analysis of synaptic phosphorylation and protein expression. *Mol. Cell. Proteomics.* **7,** 684–696
10. Cavalheiro, E. A., Naffah-Mazzacoratti, M. G., Mello, L. E., and Leite, J. P. (2006) The pilocarpine model of seizures. In *Models of Seizures and Epilepsy* (Pitkanen, A., Schwartzkroin, P. A., and Moshe, S. L., eds.), pp. 433–448, Elsevier Academic Press, London, UK
11. Mares, P., and Kubova, H. (2006) Electrical stimulation-induced models of seizures. In *Models of Seizures and Epilepsy* (Pitkanen, A., Schwartzkroin, P. A., and Moshe, S. L., eds.), pp. 153–160, Elsevier Academic Press, London, UK
12. Cline, M. S., Smoot, M., Cerami, E., Kuchinsky, A., Landys, N., Workman, C., Christmas, R., Avila-Campilo, I., Creech, M., Gross, B., Hanspers, K., Isserlin, R., Kelley, R., Killcoyne, S., Lotia, S., Maere, S., Morris, J., Ono, K., Pavlovic, V., Pico, A. R., Vailaya, A., Wang, P. L., Adler, A., Conklin, B. R., Hood, L., Kuiper, M., Sander, C., Schmulevich, I., Schwikowski, B., Warner, G. J., Ideker, T., Bader, G. D. (2007) Integration of biological networks and gene expression data using Cytoscape. *Nat. Protoc.* **2,** 2366–2382
13. Zhang, B., and Horvath, S. (2005). A general framework for weighted gene co-expression network analysis. *Stat. Appl. Genet. Mol. Biol*. **4**, Article 17
14. Horvath, S., and Dong, J. (2008). Geometric interpretation of gene coexpression network analysis. *PLoS Comput. Biol*. **4**, e1000117
15. Langfelder, P., and Horvath, S. (2008) WGCNA: an R package for weighted correlation network analysis. *BMC Bioinformatics.* **9,** 559
16. Fernandez, E., Collins, M. O., Uren, R. T., Kopanitsa, M. V., Komiyama, N. H., Croning, M. D., Zografos, L., Armstrong, J. D., Choudhary, J. S., and Grant, S. G. (2009) Targeted tandem affinity purification of PSD-95 recovers core postsynaptic complexes and schizophrenia susceptibility proteins. *Mol. Syst. Biol.* **5,** 269
17. Sheng, M., and Hoogenraad, C. C. (2007) The postsynaptic architecture of excitatory synapses: a more quantitative view. *Annu. Rev. Biochem.* **76,** 823–847
18. Greger, I. H., Ziff, E. B., and Penn, A. C. (2007) Molecular determinants of AMPA receptor subunit assembly. *Trends Neurosci.* **30,** 407–416
19. Cull-Candy, S. G., and Leszkiewicz, D. N. (2004). Role of distinct NMDA receptor subtypes at central synapses. *Sci. STKE*. **2004,** re16
20. Kim, E., and Sheng, M. (2004) PDZ domain proteins of synapses. *Nat. Rev. Neurosci.* **5,** 771–781
21. Hudmon, A., and Schulman, H. (2002) Structure-function of the multifunctional Ca2+/calmodulin-dependent protein kinase II. *Biochem. J.* **364,** 593–611
22. Owen, D. J., Collins, B. M., and Evans, P. R. (2004) Adaptors for clathrin coats: structure and function. *Annu. Rev. Cell Dev. Biol.* **20,** 153–191
23. Tada, T., Simonetta, A., Batterton, M., Kinoshita, M., Edbauer, D., and Sheng, M. (2007) Role of Septin cytoskeleton in spine morphogenesis and dendrite development in neurons. *Curr. Biol.* **17,** 1752–1758
24. Xie, Y., Vessey, J. P., Konecna, A., Dahm, R., Macchi, P., and Kiebler, M. A. (2007) The GTP-binding protein Septin 7 is critical for dendrite branching and dendritic-spine morphology. *Curr. Biol.* **17,** 1746–1751
25. Kennedy, M. B. (2000) Signal-processing machines at the postsynaptic density. *Science.* **290,** 750–754
26. Kornau, H. C., Schenker, L. T., Kennedy, M. B., and Seeburg, P. H. (1995) Domain interaction between NMDA receptor subunits and the postsynaptic density protein PSD-95. *Science.* **269,** 1737–1740
27. Huang da, W., Sherman, B. T., and Lempicki, R. A. (2009) Bioinformatics enrichment tools: paths toward the comprehensive functional analysis of large gene lists. *Nucleic Acids Res.* **37,** 1–13
28. Huang da, W., Sherman, B. T., and Lempicki, R. A. (2009) Systematic and integrative analysis of large gene lists using DAVID bioinformatics resources. *Nat. Protoc.* **4,** 44–57
29. Waung, M. W., and Huber, K. M. (2009) Protein translation in synaptic plasticity: mGluR-LTD, *Fragile X. Curr. Opin. Neurobiol.* **19,** 319–326
30. Deleted in proof
31. Li, D., Specht, C. G., Waites, C. L., Butler-Munro, C., Leal-Ortiz, S., Foote, J. W., Genoux, D., Garner, C. C., and Montgomery, J. M. (2011) SAP97 directs NMDA receptor spine targeting and synaptic plasticity. *J. Physiol.* **589,** 4491–4510
32. Elias, G. M., Funke, L., Stein, V., Grant, S. G., Bredt, D. S., and Nicoll, R. A. (2006) Synapse-specific and developmentally regulated targeting of AMPA receptors by a family of MAGUK scaffolding proteins. *Neuron.* **52,** 307–320
33. Citri, A., and Malenka, R. C. (2008) Synaptic plasticity: multiple forms, functions, and mechanisms. *Neuropsychopharmacology.* **33,** 18–41
34. Merrill, M. A., Chen, Y., Strack, S., and Hell, J. W. (2005) Activity-driven postsynaptic translocation of CaMKII. *Trends Pharmacol. Sci.* **26,** 645–653
35. Thalhammer, A., Rudhard, Y., Tigaret, C. M., Volynski, K. E., Rusakov, D. A., and Schoepfer, R. (2006) CaMKII translocation requires local NMDA receptor-mediated Ca(2+) signaling. *EMBO J.* **25,** 5873–5883
36. Zhang, Y. P., Holbro, N., and Oertner, T. G. (2008) Optical induction of plasticity at single synapses reveals input-specific accumulation of alphaCaMKII. *Proc. Natl. Acad. Sci. U.S.A.* **105,** 12039–12044
37. Li, Z., Okamoto, K., Hayashi, Y., and Sheng, M. (2004) The importance of dendritic mitochondria in the morphogenesis and plasticity of spines and synapses. *Cell.* **119,** 873–887
38. Aranda, B., Achuthan, P., Alam-Faruque, Y., Armean, I., Bridge, A., Derow, C., Feuermann, M., Ghanbarian, A. T., Kerrien, S., Khadake, J., Kerssemakers, J., Leroy, C., Menden, M., Michaut, M., Montecchi-Palazzi, L., Neuhauser, S. N., Orchard, S., Perreau, V., Roechert, B., van Eijk, K., Hermjakob, H. (2010) The IntAct molecular interaction database in 2010. *Nucleic Acids Res.* **38,** D525–D531
39. Ow, S. Y., Salim, M., Noirel, J., Evans, C., Rehman, I., and Wright, P. C. (2009) iTRAQ underestimation in simple and complex mixtures: "the good, the bad and the ugly." *J. Proteome Res.* **8,** 5347–5355